Spring 2022

Validation of ATHLET-CD with CORA-28 test

Murat Tuter

Follow this and additional works at: https://scholarsmine.mst.edu/masters_theses

Part of the Nuclear Engineering Commons

Department:

Recommended Citation

VALIDATION OF ATHLET-CD WITH CORA-28 TEST

by

MURAT TUTER

A THESIS

Presented to the Graduate Faculty of the

MISSOURI UNIVERSITY OF SCIENCE AND TECHNOLOGY

In Partial Fulfillment of the Requirements for the Degree

MASTER OF SCIENCE IN NUCLEAR ENGINEERING

2022

Approved by

Joshua Schlegel, Advisor
Ayodeji B. Alajo
Syed Alam

ABSTRACT

Following the incidents at Chernobyl and Fukushima, severe accidents at nuclear power plants (NPP) have become a global concern. These accidents generally occur because of a failure in the reactor cooling system (RCS) and result in the melting of the reactor core and fission product release. This event is mostly caused by a LOCA, loss of flow accident, station blackout or loss of heat sink. During a severe accident, generation of hydrogen as a result of steam-zircaloy fuel cladding is a significant safety concern. To better understand and prevent the hydrogen generation issue, safety related experiments and safety related codes are being developed for NPPs in various countries. The goal of this article is to simulate and analyze the CORA-28 test at KIT (formerly KfKKernforschungszentrum Karlsruhe) to confirm the capabilities of one of the safety codes, ATHLET- CD (GRS). CORA experiments were conducted to examine hydrogen production and bundle degradation for BWR and PWR type fuel bundles under accident conditions, in order to better understand the attributes and behavior of a BWR or PWR bundle during a severe accident. The CORA-28 test differs from most other CORA tests in that it was performed with a pre-oxidized BWR bundle. It was seen that temperature evolutions, the hydrogen production rates and total amount of hydrogen production predicted by ATHLET-CD closely matched the CORA-28 experiment. If operators of nuclear power plants are able to predict hydrogen generation in the containment, that will help them in avoid hydrogen explosions and strengthen NPP safety measures.

ACKNOWLEDGMENTS

I am grateful to my advisor, Dr. Joshua Schlegel, for his patience, unconditional support, advice and feedback during my MSc studies and research. I would also like to thank him for assisting me in obtaining the necessary licenses and permissions for my research.

Besides my advisor, I have a special thanks to Ministry of National Education, Republic of Turkey for rewarding me with graduate scholarship and financing my graduate education at Missouri University of Science and Technology.

I would like to express my heartfelt gratitude to Dr. Syed Alam and Dr. Ayodeji B. Alajo, members of my thesis committee, for their guidance in developing my thesis.

In addition, I would want to give special thanks to my parents, Erdogan and Selma Tuter, for giving me life in the first place and for financially and spiritually supporting me throughout my graduate studies at Missouri University of Science and Technology. Finally, I could not have completed this thesis without the support of my girlfriend, my sisters and my friends who provided stimulating discussions as well as happy distractions to rest my mind outside of my research.

TABLE OF CONTENTS

LIST OF ILLUSTRATIONS

LIST OF TABLES

NOMENCLATURE

Acronyms	Description
RCS	Reactor cooling system
LWR	Light Water Reactor
KIT	Karlsruhe Institute of Technology
GRS	Gesellschaft für Anlagen- und Reaktorsicherheit
LOCA	Loss of Coolant Accident
NPP	Nuclear Power Plant
BWR	Boiling Water Reactor
PWR	Pressurized Water Reactor
VVER	Water-Water Energy Reactor

Latin Characters	Description
α	steam void fraction (-)
w	velocity (m/s)
p	density (kg/m^3)
Ψ	interphase mass transfer rate (kg/s)
τ_i	interfacial shear per unit volume (N/m3)
H	elevation [m]
g	gravity constant (m/s^2)
S	momentum source (N/m^3)
f_{wall}	wall friction force per unit volume (N/m^3)
D	hydraulic diameter (m)

A	(flow) area [m^2]
j	superficial velocity (m/s)
q	heat flux (W/m^2)
C_o	phase distribution parameter
W	specific heat generation rate (W/m^3)
c_p	specific heat capacity at constant pressure (J/kg/K)
T	Temperature (^{o}C, K)
λ	Darcy-Weisbach friction factor (-)
	heat conductivity (W/m/K)
V	volume (m^3)
t	time (s)

Subscripts, superscripts	*Description*
V,v	vapor (or gas, resp.)
L,l	liquid
i	interphase
R,r	relative
W	wall
m	mixture
Γ	interphase mass exchange

1. INTRODUCTION

Following the Fukushima accident, many experiments were launched, and the importance of safety codes renewed for the safety of NPPs. The high concentration of hydrogen has become one of the most important NPP safety concerns since it may cause an explosion in the containment. Hydrogen arises from steam zircaloy cladding oxidation or B4C absorber oxidation with steam during a severe accident. Therefore, hydrogen accumulates in the containment, and hydrogen detonation can occur if the hydrogen concentration in the containment reaches 10%. As a result, the hydrogen content in the containment must always be kept within acceptable limits. The CORA tests were designed to understand hydrogen production and fuel degradation of a typical LWR fuel bundle under severe accident conditions.

The CORA experiments were performed between 1987 and 1993 by KIT. In total, 19 experiments were carried out with PWR, BWR, and VVER bundle configurations. Briefly, CORA experiments were electrically heated and cooled down by quenching.

The validation of the ATHLET-CD was performed with CORA-28 test. ATHLET-CD is a thermal-hydraulic based safety system code developed to understand the characteristics of NPPs under normal and accident conditions. The code was developed by the GRS. The ATHLET-CD framework is immensely modular in order to accommodate a wide range of designs and provide the best possible foundation for future growth.

1.1. RESEARCH OBJECTIVES

This research aimed to understand the characteristics of a severe accident in a nuclear power plant. The objectives of this research follow:

- Review and evaluate past severe accidents, the international severe fuel damage program, integral tests and validation methods

- Simulate the CORA-28 test facility in ATHLET-CD to evaluate the thermal hydraulic response of ATHLET-CD

- Evaluate the effectiveness of ATHLET-CD in predicting hydrogen generation phenomena during severe accidents.

1.2. LITERATURE REVIEW

This section includes a literature review of the previous well-known core degradation experiments and a review of previous CORA reports and analysis.

1.2.1. CORA Program. The first CORA test was performed in 1987 at KIT. The first report for the CORA experiments tests C and 2 was published by Hagen, Sepold, Hofmann, and Schanz (1988). The aim of these tests was to examine the behavior of the bundles with Al_2O_3 and UO_2 pellets and without absorber rods. Following this test, pre-oxidized, slow heat-up, large bundle, and dry core PWR and BWR bundle experiments were performed, and as a result, CORA experiments became a part of the International 'Severe Fuel Damage (SFD)' program. H. Austregesilo et al. [2] analyzed the QUENCH-07 experiment with ATHLET-CD and were able to plot temperature profiles quite well while hydrogen production rates were plotted at almost half of the experimental value. As well, Bestele et al. [3] calculated the CORA-13 test with ATHLET-CD and stated that the

hydrogen generation agrees well with experimental results up to the quench phase. Di Marcello et al. [4] performed the response of ATHLET-CD specifically for BWR safety in the research by investigating the CORA 16, CORA 17 and a generic German BWR plant. Depending on the modelling approximations some uncertainties were detected in the research.

1.2.2. Phebus Fission Product Program. Phebus FP tests were performed between 1993 and 2004 in order to understand PWR radioactive release in the event of a core degradation. In total, 5 tests were performed by IRSN. Figure 1.1 represents the schematic of the Phebus FP test facility. As H. Austregesilo et al. [10] mentioned in the tests cladding oxidation, fuel relocation, fission product release, fission product transport, and iodine chemistry were examined.
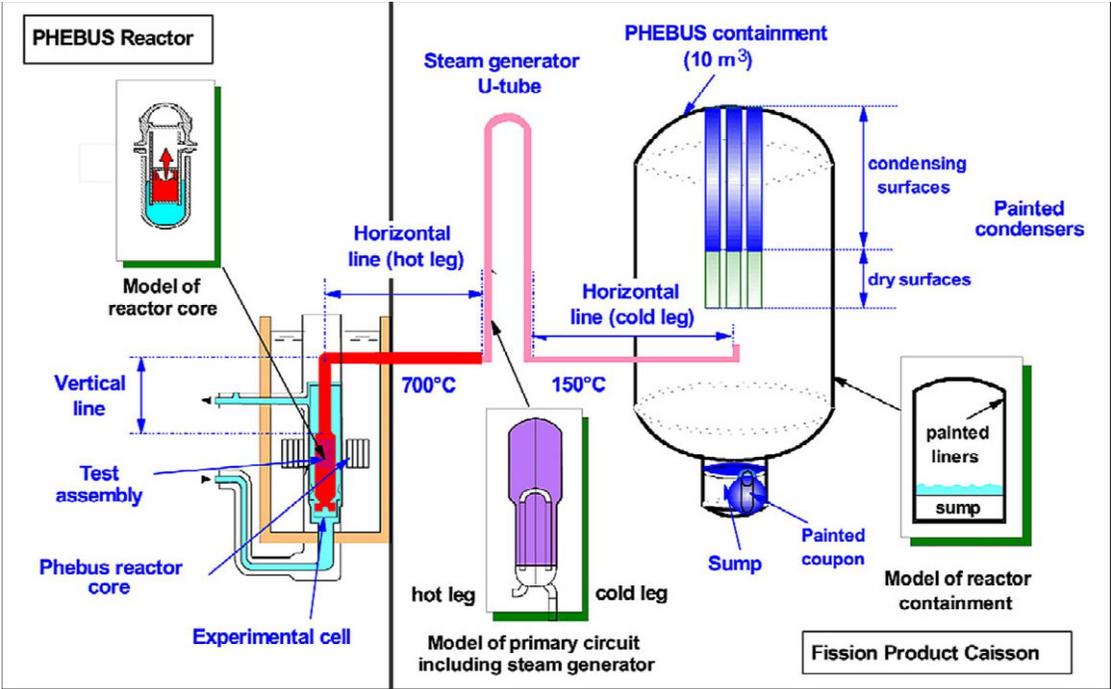
Figure 1.1 Schematic of the Phebus FP facility [9]

1.2.3. Phebus Severe Fuel Damage Program. The Phebus SFD was performed between 1986 and 1989 in order to understand the high and low oxidation on core degradation phenomena. 6 different experiments are made to study cladding oxidation and its interaction with fuel pellets, as well as the interactions between other materials. Figure 1.2 shows the representation of the Phebus SFD test train.
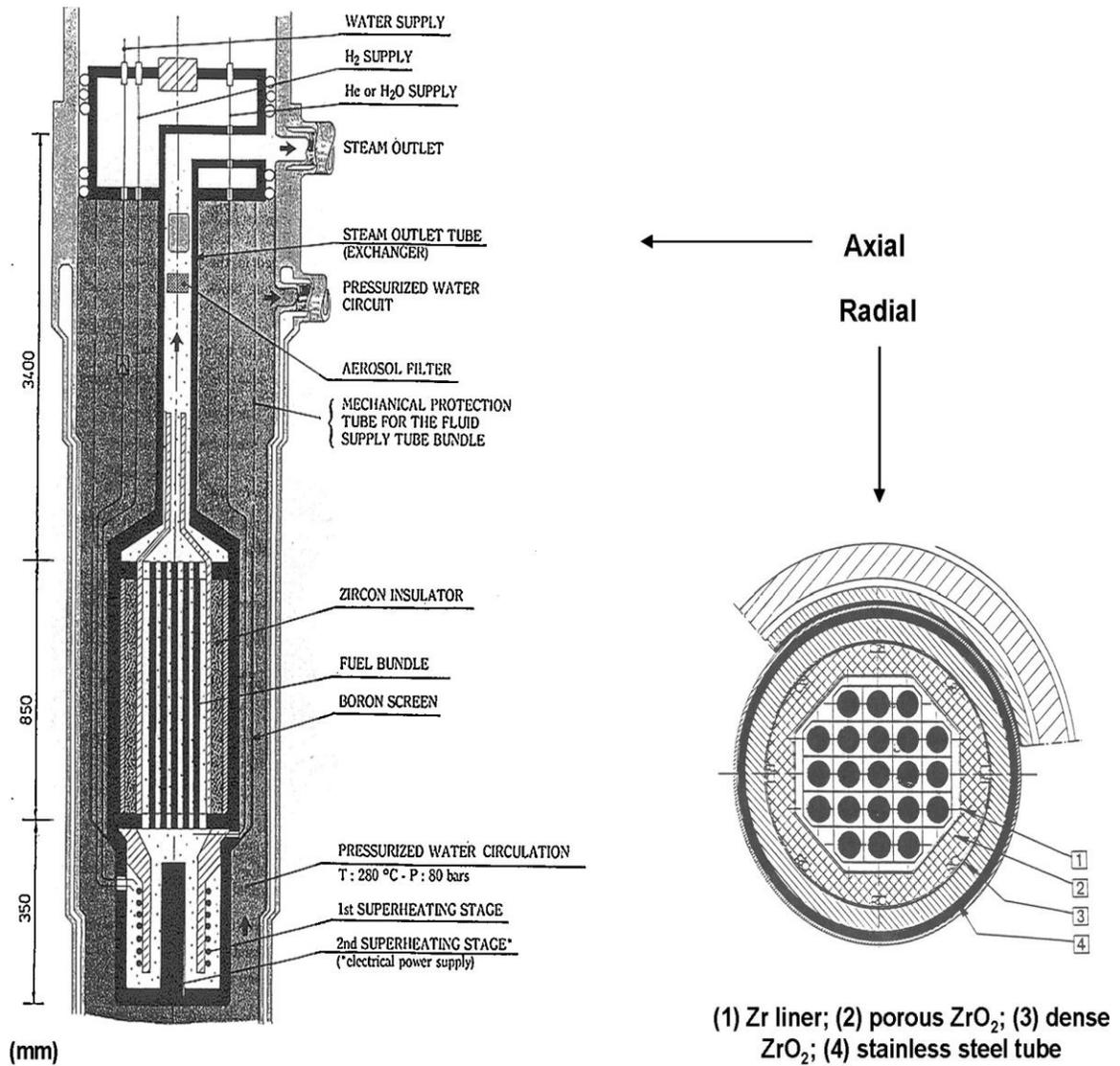
Figure 1.2 Schematic of the Phebus SFD test [9]

1.2.4. **QUENCH Program.** The experiment focused on the temperature history, hydrogen generation, cladding oxidation, and bundle degradation phenomena. The test facility in Figure 1.3 is operated with 21-31 electrically heated rods under different power and temperature conditions. 17 tests are performed as a part of the Quench experiment by KIT. Similar to CORA, the effects of reflood on the bundle degradation are being investigated.
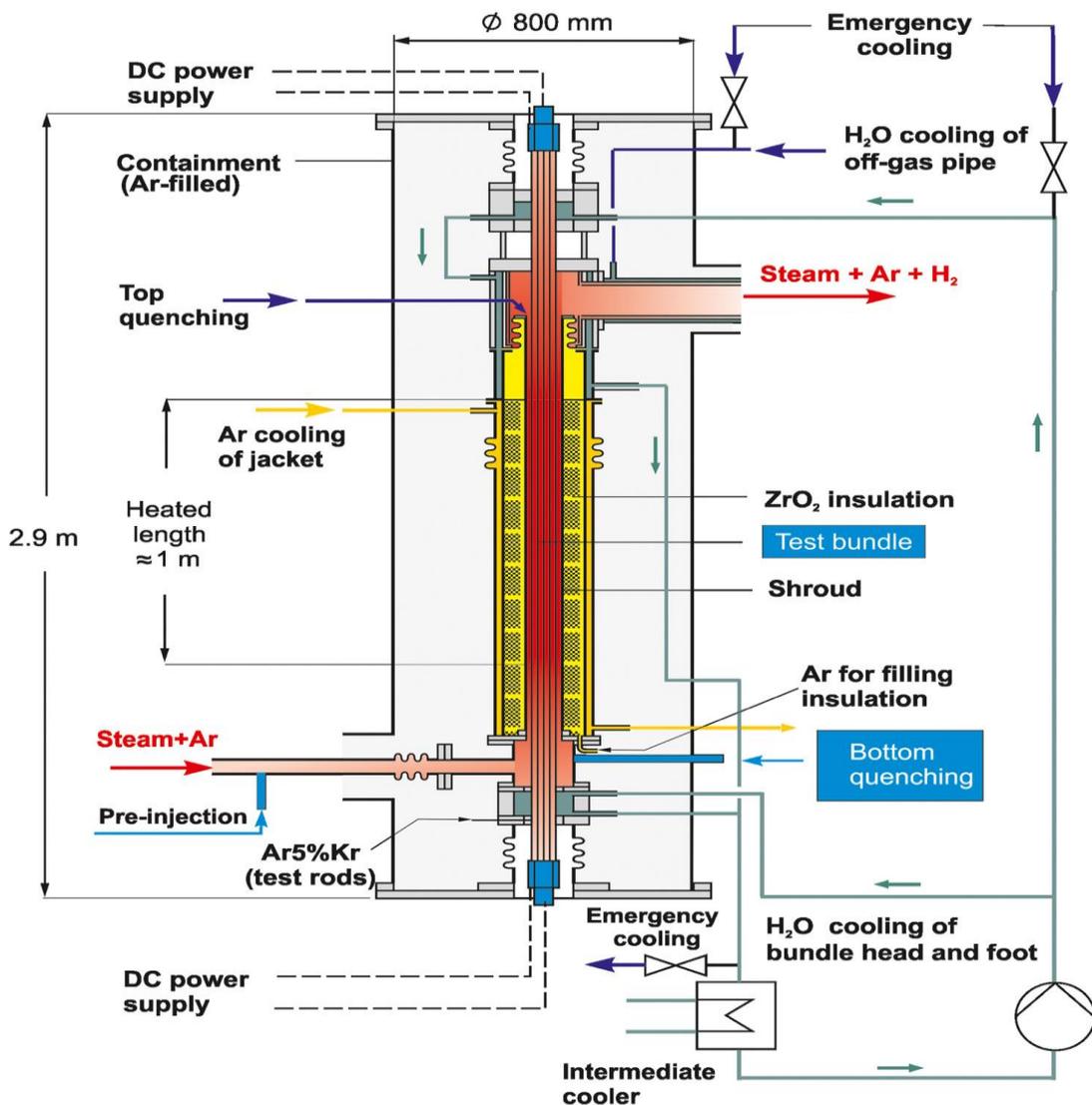
Figure 1.3 Schematic of the QUENCH test facility [13]

2. BACKGROUND

2.1. CORA-28 TEST OVERVIEW

The CORA test facilities are designed to replicate the effects of severe accident conditions on the Light Water Reactor (LWR). To provide the ideal conditions for decay heat, electrical heating was used. For both PWR and BWR type test designs, original materials were used for the bundles.

The CORA-28 test was a BWR bundle type of design. Therefore, as a fuel, original UO2 pellets with Zry-4 cladding were used. Besides that, zirconium alloy spacers, B_4C absorbers inside stainless steel tubes, and zirconium alloy channel box walls were used inside the bundle.

The schematic illustration of the CORA test facility is given in Figure 2.1. [14]. The diagram shows the configuration of the steam generator and superheater inside the containment of the CORA containment. The steam generated by the steam generator and superheated by the superheater is injected through the bottom of the bundle. The steam that is not consumed by the unit is concentrated into a condenser.

In the CORA test facility, two types of condensers are used: a vent condenser and a surge condenser. Steam that is not used by oxidation of the bundle is condensed into vent condenser units under typical working circumstances. The void volume of the surge condenser serves as a pressure suppression mechanism in the event of an emergency, due to an unusually rapid evaporation rate induced by quenching of the bundle.

The non-condensable gases are expanded and diluted in a mixing chamber to eliminate any risk of hydrogen formation during the zircaloy oxidation. Adding

compressed air to the hydrogen dilutes it to a concentration below the explosion limit. A

water-filled quench cylinder that may be adjustable electronically with a controlled speed

is located beneath the bundle [16].
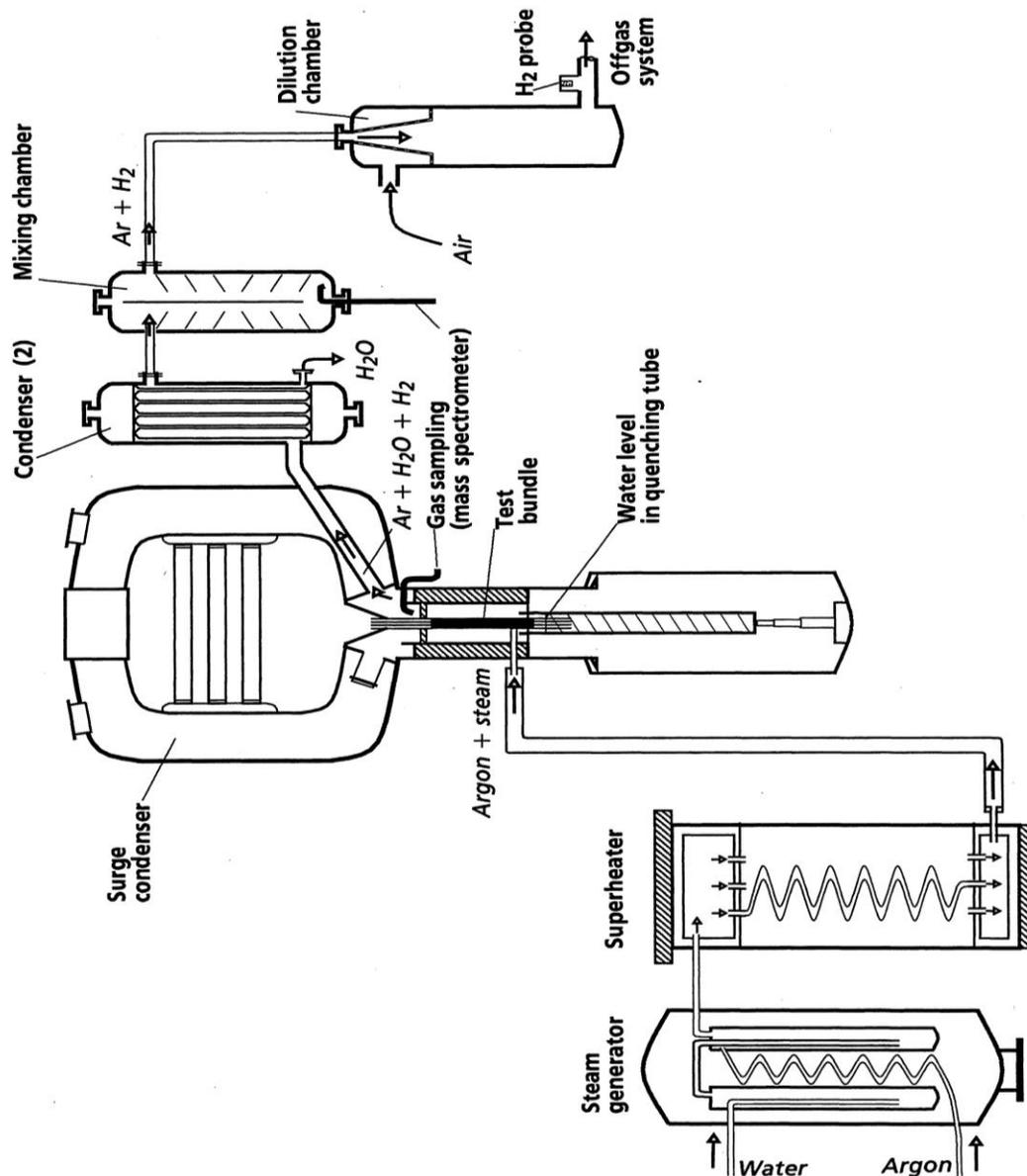
Figure 2.1 Simplified Flow Diagram of the CORA Test Facility [14]

2.1.1. Bundle Design. Rod arrangement and Rod types used in CORA-28 experiment are shown in Figure 2.2 and Figure 2.3. To represent a BWR fuel arrangement, the bundle included 12 heated rods, 6 unheated rods, two channel box walls and the absorber blade.[1]
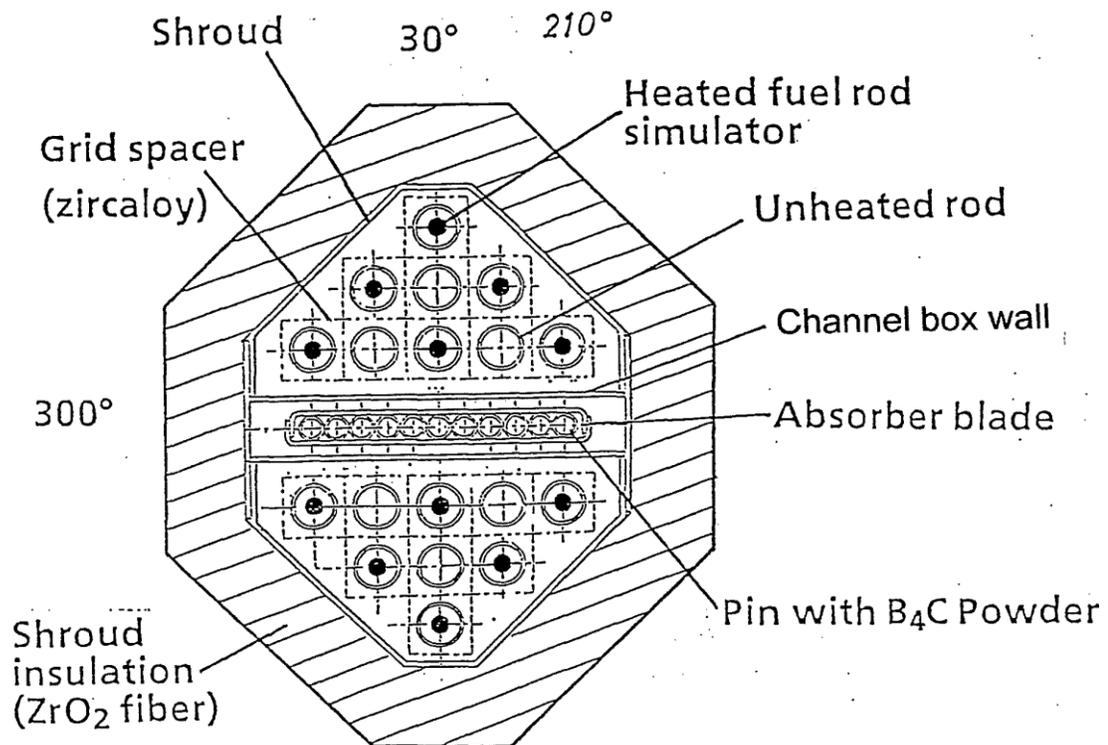
Figure 2.2 Rod arrangement of bundle CORA-28 experiment [1]

The heated rod contains a Zircaloy-4 cladding tube and uranium dioxide pellets. The heater is made of tungsten rod where the electrodes on it are made of molybdenum and copper. Solid UO_2 pellets and zircaloy cladding were used to make unheated rods in the bundle. The channel box walls include Zircaloy-4 and the absorber blade consists of stainless steel and B_4C. The bundle is enclosed by a high temperature shield to guarantee

a uniform radial temperature distribution and to keep the heat loss as low as possible.

Shield is made of zirconium dioxide and aluminum oxide. During the test, high

temperature thermocouples were used to determine the temperature of the bundles.
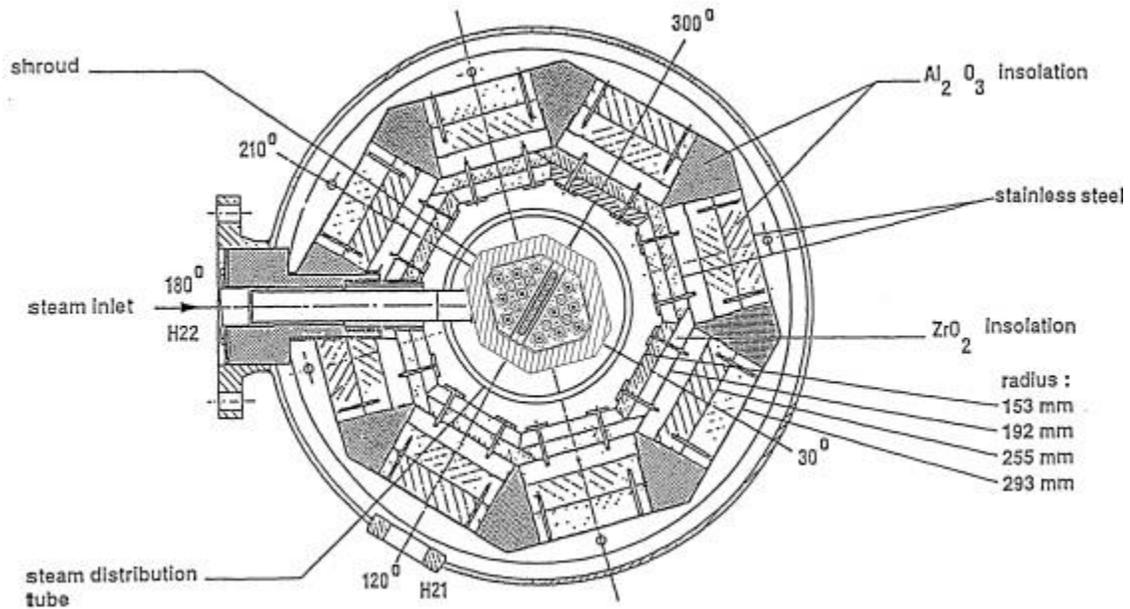
Figure 2.3 Horizontal cross section of the high temperature shield [17]

2.1.2. Test Conduct. The CORA-28 test includes 4 different phases. Since the aim

of the CORA-28 experiment is to investigate the influence of pre-oxidation on a BWR

type bundle, pre-oxidation was applied to the CORA test facility in this experiment. The

pre-oxidation phase from Figure 2.4 to Figure 2.7 and post-test phase from Figure 2.8 to

Figure 2.11 represents the amount of argon flow, steam input, power input, and system

pressure applied to the system.
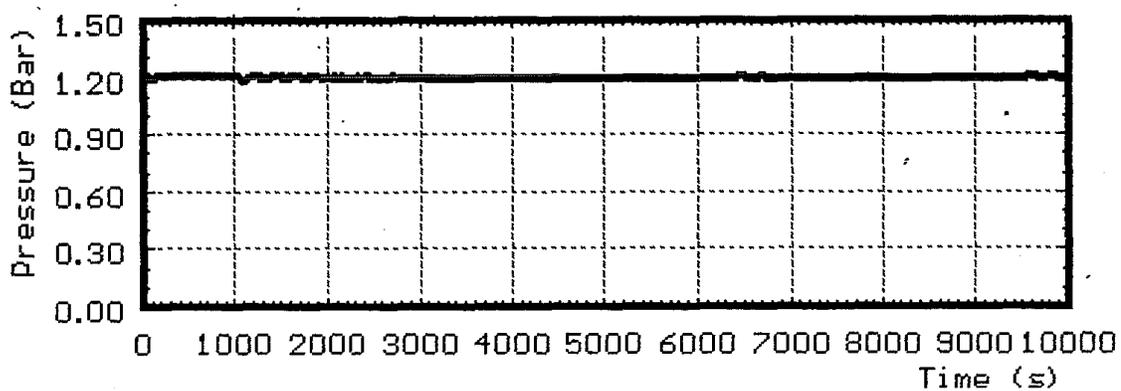
Figure 2.4 System Pressure(gauge) of CORA-28 in peroxidation phase [1]
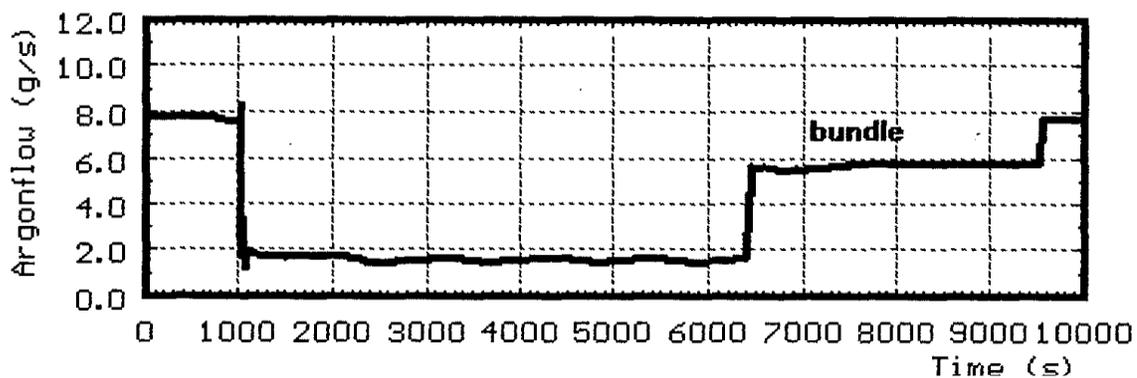
Figure 2.5 Argon Flow of CORA-28 in peroxidation phase [1]
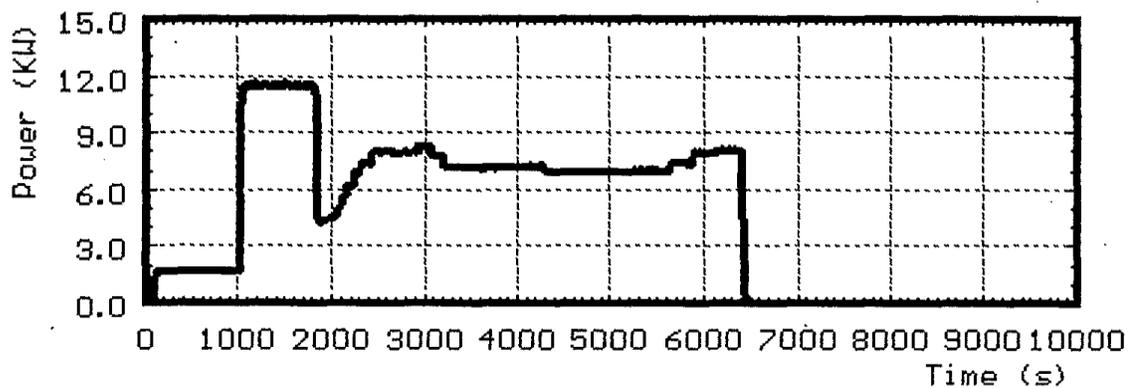
Figure 2.6 Power input of CORA-28 in peroxidation phase [1]
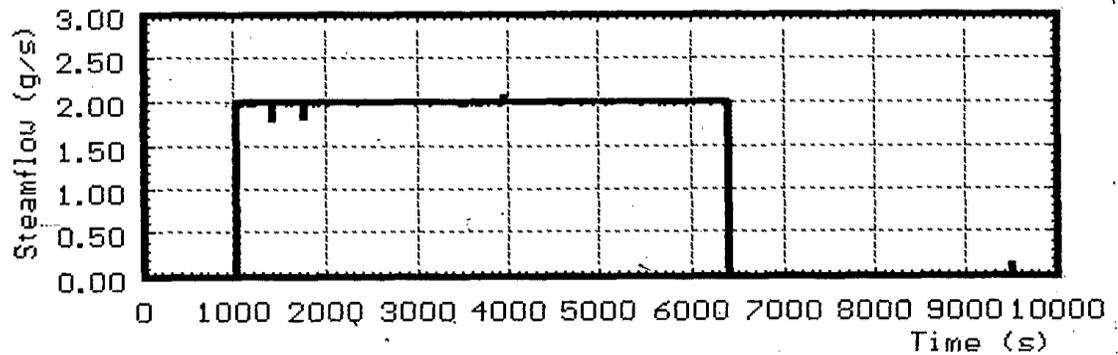
Figure 2.7 Steam Flow of CORA-28 in peroxidation phase [1]

For the test sequence of CORA experiments, phases are separated as;

0-3000 seconds: pre-heating

3000-4800 seconds: transient

After 4800 seconds: cooldown.

System pressure and argon flow through the bundle are constant and the amounts are 120 kilopascals and 8 g/s. During the pre-heat phase, a power input close to zero is applied. Argon gas was used to heat fuel bundle with 770 K temperature.

The transient phase is where accident conditions get started. To be able to provide an accident condition where water boils and becomes steam and then interacts with zircaloy cladding, which results in hydrogen production, in transient phase 2 g/s is steam added to the system, and from 4.5 to 23 kW of electric power is applied to create an initial temperature increase.

In cool-down phase, the test was terminated by turning off the electric power and stopping steam addition at 4800 s to be able to create the function of emergency core cooling system in a NPP and to slow down accident condition.
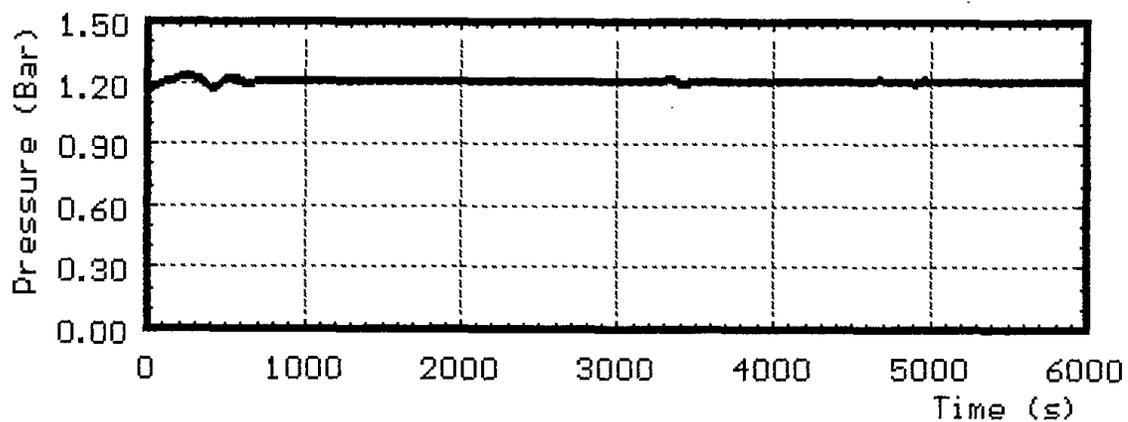
Figure 2.8 System overpressure of CORA-28 [1]
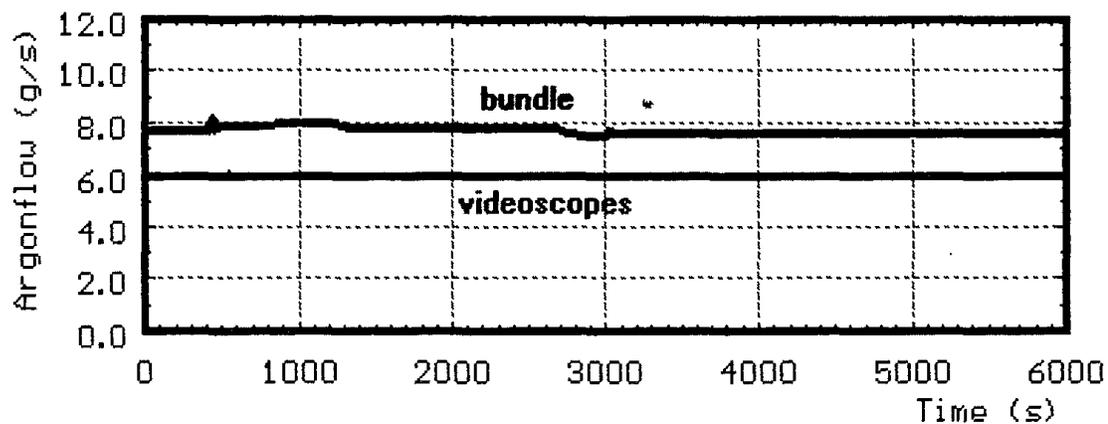
Figure 2.9 Argon flow of CORA-28 experiment [1]
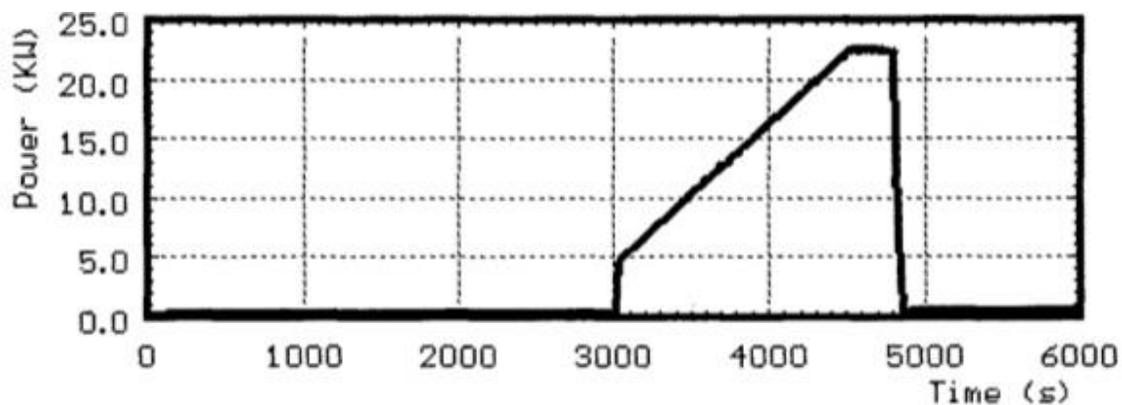
Figure 2.10 Power input of CORA-28 experiment [1]
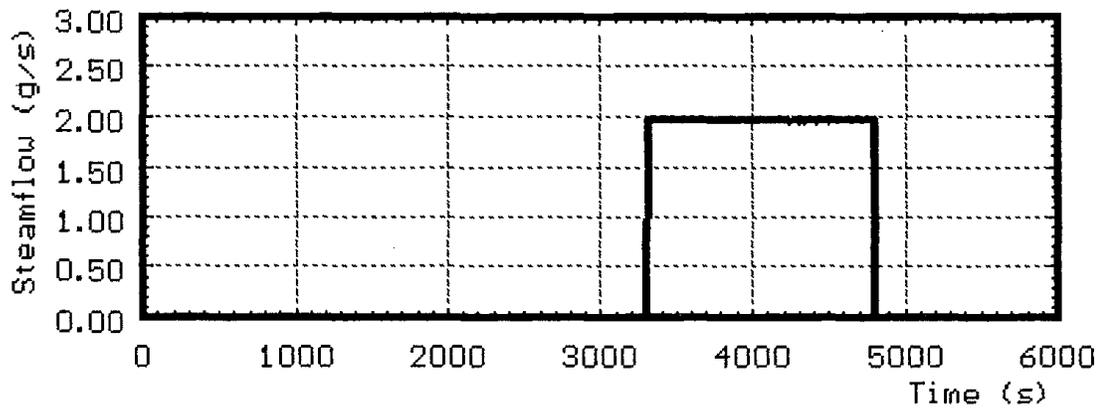
Figure 2.11 Steam input of CORA-28 experiment [1]

2.1.3. Design Characteristic of Bundle CORA-28. The Table 1.1 represents the design characteristics of CORA-28 test facility.

Table 1.1. Design characteristics of bundle CORA-28 [1]

Bundle Type		BWR
Bundle Size		18 rods
Number of heated rods		12
Number of unheated rods		6
Pitch		14.3 mm
Rod outside diameter		10.75 mm
Cladding material		Zircaloy-4
Cladding thickness		0.725 mm
Rod length	Heated rods elevation	1840 mm
	Unheated rods elevation	1672 mm

Table 1.1. Design characteristics of bundle CORA-28 [1] (cont.)

Heated pellet stack		0 to 1000 mm
Heater material		Tungsten (W)
Heater	Length	1000 mm
	Diameter	6 mm
Fuel pellets	Heated rods	UO_2 annular pellets
	Unheated rods	UO_2 fuel pellets
Pellet stack	Heated rods	0 to 1000 mm
	Unheated rods	-200 to 1300 mm
U-235 enrichment		0.2 %
Pellet outer diameter(nominal)		9.1 mm
Grid spacer	Material	Zircaloy -4
	Length	42 mm
	Location(upper end)	Lower -33 mm
		Center 578 mm
		Top 1167 mm
Shroud	Material	Zircaloy -4
	Wall thickness	1.2 mm
	Outside dimensions	94.4 x 116 mm
	Elevation	40 -1235 mm
Shroud insulation	Material	ZrO_2 fibre
	Insulation thickness	19 mm

Table 1.1. Design characteristics of bundle CORA-28 [1] (cont.)

	Elevation	40 mm to 1070 mm
Cu electrode	Length	189 mm(lower end)
	Length	669 mm(upper end)
	Diameter	8.6 mm
Absorber rod	Number of rods	11
	Material	B_4C powder
	Cladding	Stainless Steel
	Cladding OD	5.8 mm
	Cladding ID	4.6 mm
	Length	1600 mm
	Absorber material	-270 mm to 1300 mm
Absorber blade	Material	Stainless steel
	Dimensions inside	76 x 6 mm
	Wall thickness	1 mm
[box wall	Material	Zircaloy -4
	Dimensions inside	13 x 92 mm
	Wall thickness	1.2 mm
Plenum Volume	Heated rods	19.8×10^{-6} m^3
	Unheated rods	39.0×10^{-6} m^3

2.2. OVERVIEW OF ATHLET-CD

ATHLET is a thermal-hydraulic computer code developed by GRS for normal and abnormal operational conditions in a nuclear power plant. The code is written in Fortran. The aim of the ATHLET is to understand the characteristics of a nuclear power plant during design basis accidents for PWRs, BWRs, SMRs, and Gen IV reactors. For accidents with core degradation, ATHLET-CD has been implemented as an extension of ATHLET. ATHLET-CD helps to understand core damage progression, fission product release and aerosol behavior during severe accidents to improve accident management measures. Therefore, ATHLET-CD is a sub module of ATHLET and uses the same input deck. The range of applicability of the ATHLET for the working fluids is light and heavy water, sodium, helium, non-boiling fluids (liquid lead, molten salts, lead-bismuth eutectic), and user-provided fluids [8].

The structure of the ATHLET-CD is shown in Figure 2.12. Basically ATHLET-CD = ATHLET + special modules. L. Lovasz et al. noted that "The rod module ECORE consists of models for fuel rod, absorber rod (AIC and B4C) and the fuel assembly including BWR canister and absorber" [7]. The FIPREM module simulates the fission product release. ATHLET/ATHLET-CD can be coupled with the containment analysis code COCOSYS [2].

The code follows four different steps in order to make a calculation;

1. Input

2. Initialization

3. Steady-state calculation

4. Transient calculation.
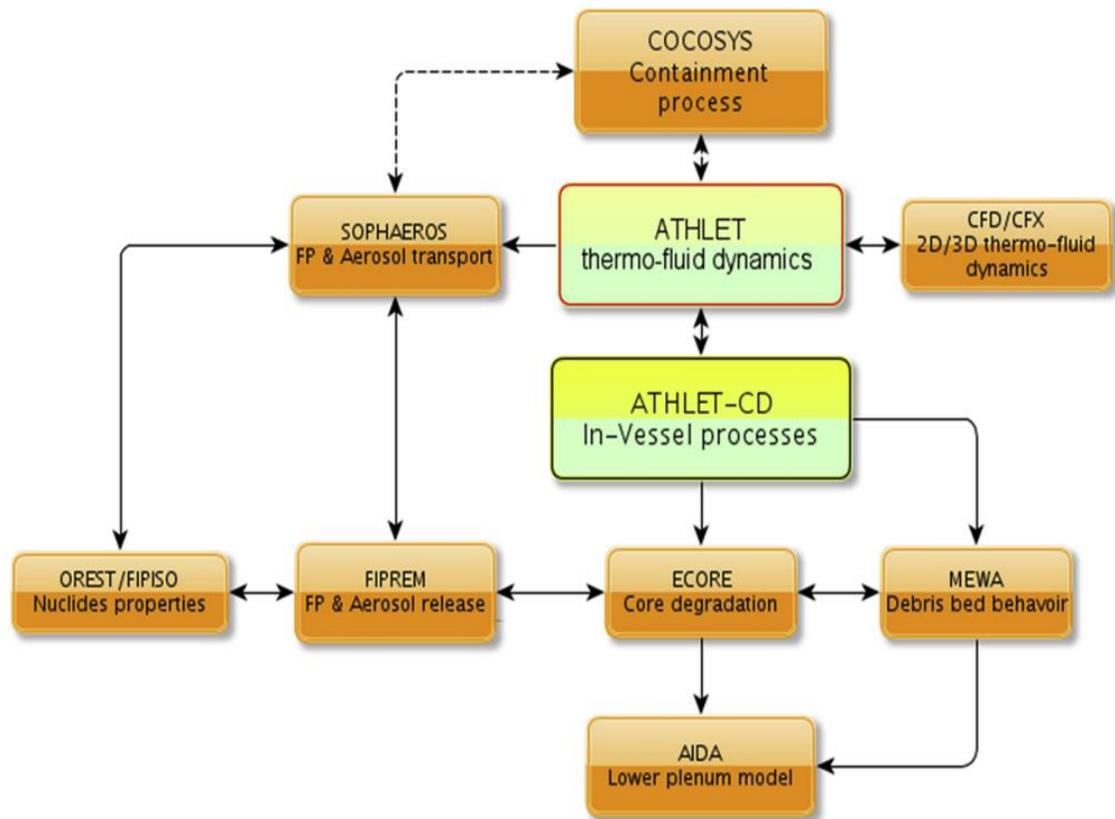
Figure 2.12 The structure of ATHLET-CD [12]

The ordinary differential equations in the system are solved fully implicitly by the numerical integration method or FEBE module. The most necessary module is the thermo-fluid dynamic module, which includes two different types of fluid-dynamics equation systems [2]. The 6-equation model or two fluid model takes into consideration fully separated conservation equations for liquid and vapor mass, energy and momentum. The 5-equation model uses separate conservation equations for liquid and vapor mass and energy with a mixture momentum equation [8].

3.METHODS

3.1. NODALIZATION WITH ATHLET-CD

Figure 3.1. represents the nodalization of the CORA bundle within ATHLET-CD. The nodalization includes 55 control volumes for thermo-fluid objects and 26 control volumes for heat conduction objects. Nodes are divided into different numbers of control volumes to represent different initial conditions such as temperature, pressure, flow rates, etc. in the object. The nodalization includes the bundle, flow channels, bypass, shroud, shield and junctions for steam inlet, argon inlet, etc. inlet. Steam and argon junctions are placed in the bottom bundle.
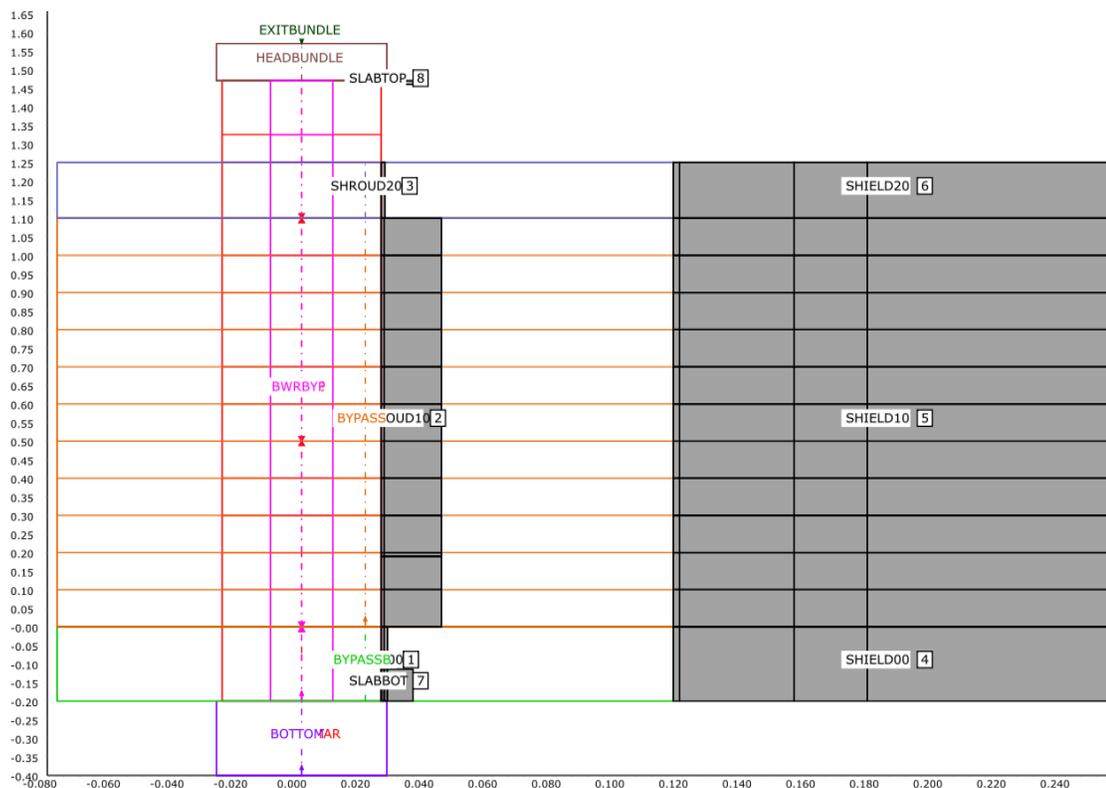
Figure 3.1 Nodalization scheme

As Di Marcello et al. modelled the QUENCH test facility, "The thermal hydraulic behavior between the absorber blade and the bundle is taken into account by means of BYPASS, as well as the annular space between the shroud and the HTS is simulated by BYPASS" [4]. Modeling with ATHLET-CD has one drawback: only one heat object for the fuel rods can be applied. Therefore, the code allows modelling fuel rods as only heated or unheated rods. In order to account for heat transfer via conduction, convection, and radiation, the high temperature shield and shroud are included in the model as standard heat conduction objects.

3.2. MODULES

ATHLET and ATHLET-CD include various modules which help to simulate accident conditions. The thermal behavior of debris bed and the molten pool, the fission product release from the fuel rods and the transport are not considered in the simulations as well as 'CORA-07' sample in ATHLET's interface [6]. The modules used in this research are;

3.2.1. Thermo-Fluid Dynamic Module. The thermo-fluid dynamic TFD module is the main module of ATHLET which includes the input data of thermo-fluid objects. This module performs an initial thermal hydraulic state for steady state calculation, controls the data exchange and provides data to other modules. The thermal-hydraulic state of the system is represented with partial different equations that depend on time and space. Generally, the core degradation modules are coupled with the 5 equation TFD module. Bestele et al. stated that "ATHLET contains the conservation laws for vapor mass, liquid mass, vapor energy, liquid energy and overall momentum" [3].

liquid mass:

$$\frac{\partial((1-\alpha)p_L)}{\partial t} + \nabla \cdot \left((1-\alpha)\vec{w}_L p_L\right) = -\Psi$$

vapor mass:

$$\frac{\partial(\alpha \cdot p_V)}{\partial t} + \nabla \cdot (\alpha \cdot \vec{w}_v p_V) = \Psi$$

liquid energy:

$$\frac{\partial[(1-\alpha)\rho_L(h_L + \frac{1}{2}\vec{w}_L\vec{w}_L - \frac{p}{\rho_L})}{\partial t} + \nabla \cdot \left((1-\alpha)p_L\vec{w}_L(h_L + \frac{1}{2}\vec{w}_L\vec{w}_L)\right) = -\rho\frac{\partial(1-a)}{\partial t}$$

$+ \vec{\tau_i}\vec{w}_L$ shear work at the phase interface

$+ (1-\alpha)\vec{\tau_i}(\vec{w}_v - \vec{w}_L)$ dissipation due to interfacial shear

$+ (1-\alpha)\rho_L\vec{g}\vec{w}_L$ gravitational work

$+ \dot{q}_{wL}$ heat flow through structures

$+ \dot{q}_i$ heat flow at the phase interface

$+ \Psi\left(h_{\Psi,L} + \frac{1}{2}\vec{w}_\psi\vec{w}_\psi\right)$ energy flow due to phase change

$+ S_{E,L}$ external source terms

where

$\vec{w}_\psi = \vec{w}_L$ for evaporation

$\vec{w}_\psi = \vec{w}_v$ for condensation

vapor energy:

$$\frac{\partial[\alpha\rho_V h_V + \frac{1}{2}\vec{w}_V\vec{w}_V - \frac{\rho}{\rho_V}]}{\partial t} + \nabla \cdot [\alpha\rho_V\vec{w}_V(h_V + \frac{1}{2}\vec{w}_V\vec{w}_V)] = -\rho\frac{\partial a}{\partial t}$$

$- \vec{\tau_i}\vec{w}_L$ shear work at the phase interface

$+ \alpha\vec{\tau_i}(\vec{w}_v - \vec{w}_L)$ dissipation due to interfacial shear

$+ \alpha \rho_v \vec{g} \overrightarrow{w}_v$ gravitational work

$+ \dot{q}_{wv}$ heat flow through structures

$+ \dot{q}_i$ heat flow at the phase interface

$+ \Psi \left(h_{\Psi,v} + \frac{1}{2} \overrightarrow{w}_\psi \overrightarrow{w}_\psi \right)$ energy flow due to phase change

$+ S_{E,V}$ external source terms

$\overrightarrow{w}_\psi = \overrightarrow{w}_L$ for evaporation

$\overrightarrow{w}_\psi = \overrightarrow{w}_v$ for condensation

liquid momentum:

$$\frac{\partial[(1-\alpha)\rho_L \overrightarrow{w}_L]}{\partial t} + \nabla\big((1-\alpha)\rho_L \overrightarrow{w}_L \overrightarrow{w}_L\big) + \nabla \cdot \big((1-\alpha)p\big) =$$

$+ p\nabla \cdot (1 - \alpha)$ interfacial pressure term

$+ \vec{\tau}_i$ interfacial friction

$-(1-\alpha)\overrightarrow{f_w}$ wall friction

$-\psi \vec{w}_\Gamma$ momentum flux due to phase change

$-(1-\alpha)\rho_L \vec{g}$ gravitation

$+\alpha(1-\alpha)(\rho_L - \rho_v)\vec{g} D_h \nabla_\alpha$ water level force

$+\alpha(1-\alpha)\rho_m \cdot \left(\frac{\partial \overrightarrow{w}_R}{\partial t} + \overrightarrow{w}_v \nabla \overrightarrow{w}_v - \overrightarrow{w}_l \nabla \overrightarrow{w}_l\right)$ virtual mass

$+ S_{I,L}$ external momentum source terms

vapor momentum:

$$\frac{\partial[\alpha \rho_V \overrightarrow{w}_V]}{\partial t} + \nabla(\alpha \rho_V \overrightarrow{w}_V \overrightarrow{w}_V) + \nabla \cdot (\alpha \, p) =$$

$+ p\nabla \cdot \alpha$ interfacial pressure term

$- \vec{\tau}_i$ interfacial friction

$-\alpha\overrightarrow{f_w}$ wall friction

$+\psi\overrightarrow{w_\Gamma}$ momentum flux due to phase change

$-\alpha\rho_v\vec{g}$ gravitation

$-\alpha(1-\alpha)(\rho_L-\rho_v)\vec{g}D_h\nabla_\alpha$ water level force

$+\alpha(1-\alpha)\rho_m\cdot(\frac{\partial\overrightarrow{w_R}}{\partial t}+\overrightarrow{w_v}\nabla\overrightarrow{w_v}-\overrightarrow{w_l}\nabla\overrightarrow{w_l})$ virtual mass

$+S_{I,V}$ external momentum source terms(e.g. pumps)

where:

$$\rho_m = \alpha\rho_V + (1-\alpha)\rho_L$$

$$\overrightarrow{w_R} = \overrightarrow{w_v} - \overrightarrow{w_L}$$

Overall momentum equation for the two-phase mixture:

$$\frac{\partial(\rho_m\overrightarrow{w_m})}{\partial t} - \overrightarrow{w_m}\frac{\partial\rho_m}{\partial t} + \rho_m\overrightarrow{w_m}\nabla\overrightarrow{w_m} + \nabla\left(\alpha(1-\alpha)\frac{\rho_V\rho_L}{\rho_m}\overrightarrow{w_R}\overrightarrow{w_R}\right) + \nabla_p =$$

$\overrightarrow{f_w}$ wall friction

$\rho_m\vec{g}$ gravitation

$+S_{I,m}$ external momentum source terms

where

$$\overrightarrow{w_m} = \frac{1}{\rho_m}(\alpha\rho_V\overrightarrow{w_v}+(1-\alpha)\rho_L\overrightarrow{w_L})$$

The relative velocity between liquid and vapor is determined by a drift-flux model [3].

The general relationship of the drift-flux theory is given by

$$<<w_v>> = C_0<j> +<<w_{vj}>>$$

where

$$<< w_v >> = \frac{< j_v >}{< \alpha_v >} = \frac{\frac{1}{A} \int_0^A j_v \, dA}{\frac{1}{A} \int_0^A \alpha_v \, dA}$$

and
$$< j > = < j_v > + < j_L >$$

This relationship can be recast to give the drift-flux $< j_{vL} >$ explicitly.

3.2.2. Heat Conduction and Heat Transfer Module. The HECU module is a one-dimensional module which offers a Fourier equation solution for simulating temperature profiles and energy transmission of solid objects. The code neglects the pressure effects on the material's density, heat conductivity, heat capacity and properties.

The conservation of energy in a control volume is used to calculate the heat conduction equation:

$$\int_V W \cdot dV \;\; = \;\; c_\rho \cdot \rho \cdot \int_V \frac{\delta T}{\delta t} \cdot dV + \;\; \int_S \vec{q} \, dA$$

Rate of heat   Rate of change of   heat flow crossing

Generation   internal energy   the boundary

Then the heat flow can be described by the equation:

$$\int_S \vec{q} \, d\vec{A} = \lambda \cdot \int_S grad \, T \cdot d\vec{A}$$

Observing the Gaussian rule, the right side of the equation can be transformed:

$$-\lambda \cdot \int_S grad \, T \cdot d\vec{A} = -\lambda \int_V div \, (grad \, T) \cdot dV = -\lambda \int_V \nabla^2 T \cdot dV$$

Substituting the equation above into the first equation

$$\int_V W \cdot dV = c_\rho \cdot \rho \cdot \int_V \frac{\delta T}{\delta t} \cdot dV - \lambda \int_V \nabla^2 T \cdot dV$$

$$\frac{\delta T}{\delta t} = \frac{\lambda}{c_\rho \cdot \rho} \nabla^2 T + \frac{1}{c_\rho \cdot \rho} \cdot W$$

This differential equation is the well-known Fourier equation.

3.2.3. Time Integration Module. FEBE (Forward Euler, Backward Euler) is a general-purpose solver for the solution of non-linear ODE systems of first order. It is based on an Euler method with backward difference. The main characteristics are:

· One-step method of variable order

· Explicit / implicit partitioning of the ODE system

· Automatic time step control

· Automatic choice of error order (max. 3)

· Rigorous error control through an extrapolation technique

· Numerical linearization of the equation system

· Application of the sparse matrix solver FTRIX

· Automatic control of the Jacobian matrix update

· Interfaces to the models

· for additional time step reduction

· for additional Jacobian updates

· for error bounds dedicated to the different types of solution variables [5].

3.2.4. Rod Plug Module. Mass per unit length (kg/m) for lower and upper plug data is defined in this section.

3.2.5. Electrical Heater Rod Module. Since the CORA test has electrically heated rods, this data is placed in the code. This is the section where the radius, resistance and material properties are defined for the electrical heater rod.

3.2.6. Emissivity Module. All emissivity data is defined in this section for each side of the core.

3.2.7. Rod Oxidation Module. Zirconium oxidation is simulated in this module with 3 different models provided for users. The Leistikow correlation model is used for the modelling of the test facility since it performs the widest temperature range for oxidation.

3.2.8. Mechanical Rod Behaviour Module. Mechanical rod behavior module starts the mechanical rod behavior model, including ballooning, internal rod pressure, and cladding burst calculation.

3.2.9. Rod Relocation Module. This module describes the liquefaction and relocation of cladding and fuel. All the recommended material data refers to Zry-2/4 from NUREG/CR-6150.

3.2.10. BWR Absorber Rod Module. Since CORA-28 is a test facility with a BWR bundle, to define the absorber rod's thickness, width, number and same properties for channel box wall and absorber blade, this module is inserted for simulation.

3.2.11. Material Property Table Names. The ATHLET or ATHLET-CD by itself, doesn't have a library for the properties of material. In this section, heat conductivity, density, and heat capacity of UO_2, zircaloy, stainless steel and boron carbide are added for different temperatures.

4. RESULTS

The main results of the ATHLET-CD calculation are displayed in Figure 4.1-4.8 with the corresponding experimental values. Temperature profiles as a function of time are shown in the figures. The temperature rise caused by the zirconium steam oxidation reached around 150 mm at the lower end and 1250 mm at the upper end. The preheated gas and steam entered the bundle at 0 mm elevation. For up to 3000 seconds, bundle was mostly heated by the temperature of the incoming argon gas, which was around 770 K. As expected, that caused a slight increase in temperature profiles in ATHLET-CD. At 3000 seconds, the injection of steam and an increase in electric power cause the temperature to rise. Therefore, a sharp increase was detected in temperature profiles up to 4800 seconds in ATHLET-CD. After all, at 4800, seconds a sharp decrease in temperature profile was detected since quenching or cooling started in this time interval. This phase is the representation of an emergency core cooling system in the NPP.
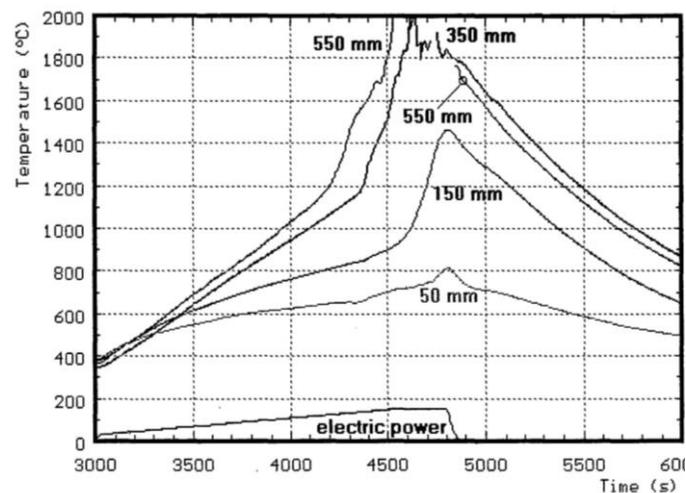

Figure 4.1 Temperature of heated rods obtained during CORA-28 experiment between 50-550 mm [1]
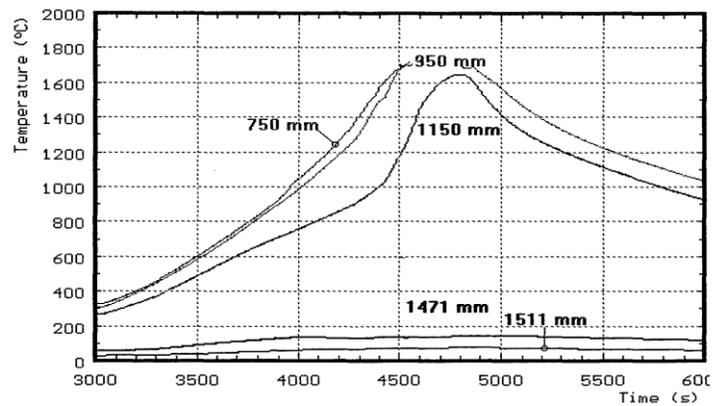
Figure 4.2 Temperature of heated rods obtained during CORA-28 experiment between 750-1500 mm [1]

The temperature profiles didn't match for the top of the bundle and the bottom of the bundle. Also in the experiment, argon and steam are injected from the left bottom side of the bundle. In this research's nodalization, steam and argon are placed as a junction from the bottom of the bundle which caused these differences.
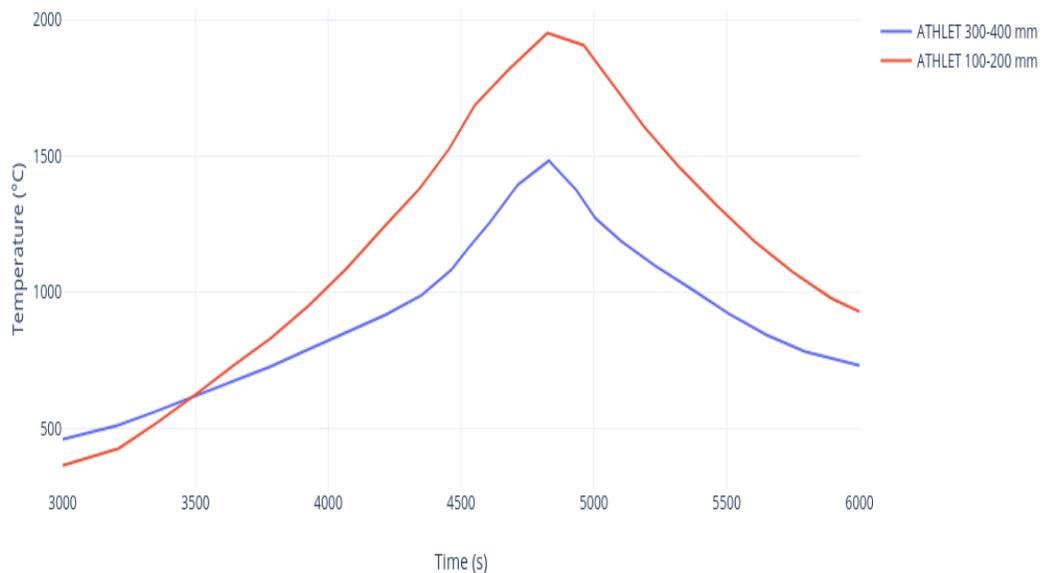
Figure 4.3 Temperature of heated rods in ATHLET-CD

For the top side, the temperature of the bundle did not exceed 200 degrees Celsius in the experiment. Because the head bundle has an additional cooling system with argon gas. In this research, the head bundle cooling is neglected.

Shroud temperature and bundle temperature showed close results because of the shroud insulation's heat capacity and insulation properties in the experimental results. In ATHLET, shroud temperature increased proportionally with respect to bundle temperature, and the temperature of the shroud insulation is given in Figure 4.4.

Figure 4.4 Temperature in shroud insulation

Figure 4.5 Heater power in ATHLET-CD

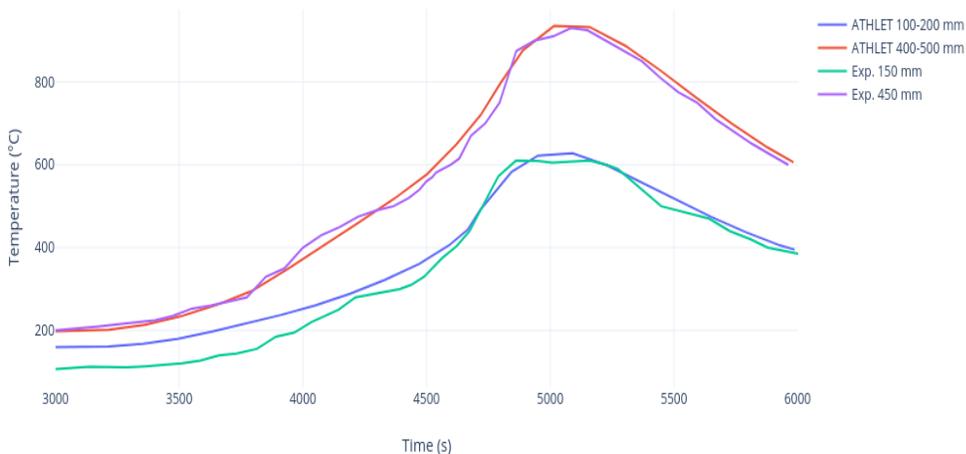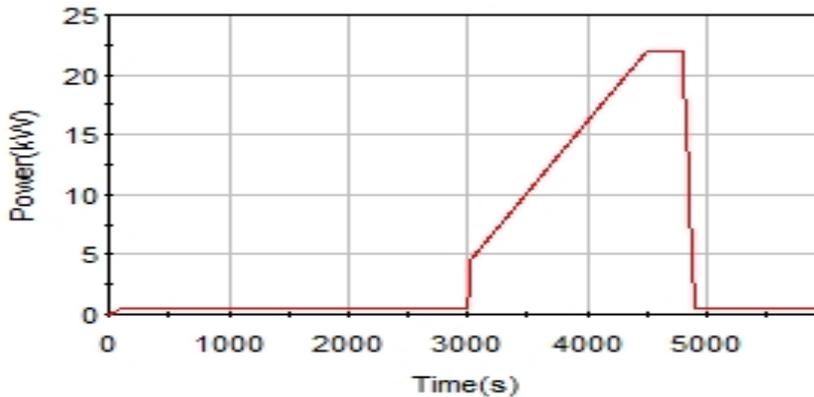Figure 4.7 shows the hydrogen production rates for the experiment and for the obtained results from ATHLET-CD. In the experimental results for hydrogen production, two different lines are plotted as corrected and measured. During the experiment, to be able to measure the delay time of the monitoring gas, a calibration test was made with the CORA-7 test bundle [15]. This delay time of monitoring gas applied for hydrogen production in all CORA experiments. In the end, a lower than expected hydrogen production rate was observed. Therefore, the measured data is updated according to the actual gas concentration. New values are presented as corrected values. Therefore, in this research, corrected values are taken into consideration for comparison. Since the increase in the heater power starts around 3000 seconds and the injection of high temperature water steam starts around 3200 seconds, melt formation and zirconium steam reaction are expected to be observed after 3200 seconds.
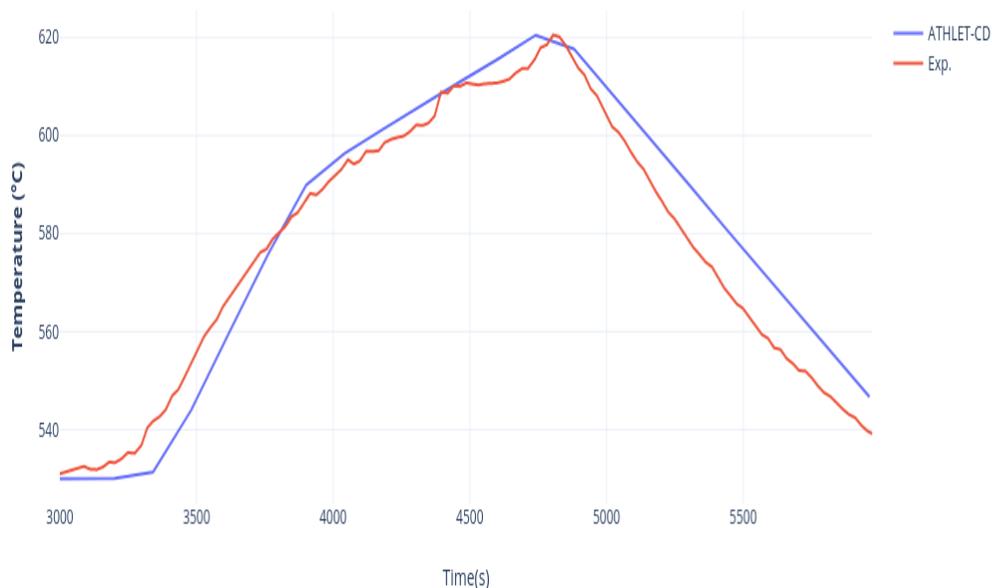

Figure 4.6 Temperatures at steam inlet

During the experiment, hydrogen production started around 4000 seconds and the ATHLET-CD's result showed hydrogen production onset around 600 seconds earlier than experimental conditions. The reason is caused by the challenges faced in modelling the zirconium oxidation model. In Figure 4.7, The hydrogen production rate plotted by the code, reaches a peak just before the cool-down phase like in the experiment in Figure 4.7. The reason is that the quenching started at 4800 seconds, which led to significantly more hydrogen being produced as a result of a larger volume of steam arising from the evaporation of water in contact with the heated cladding surface.

Figure 4.7 Hydrogen production rate
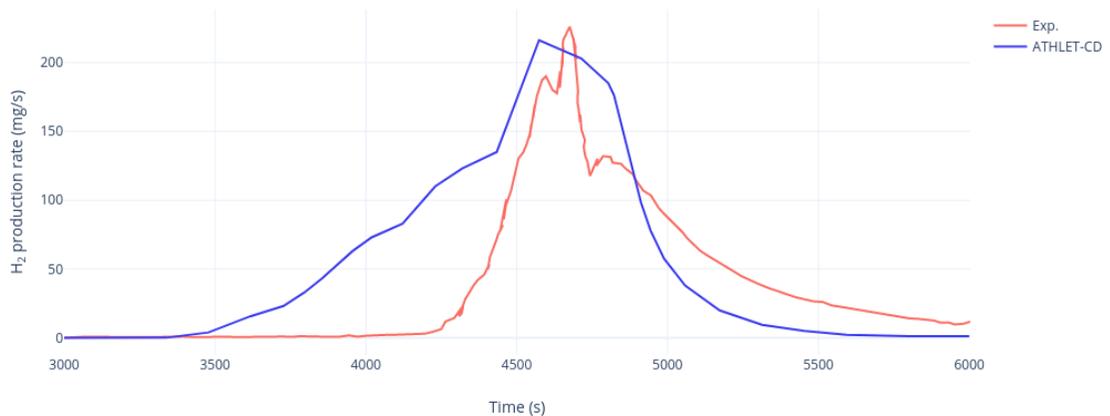
The total amount of hydrogen produced by the code is 105 grams and the total amount of hydrogen produced during the experiment is 104 grams. The maximum production rate for both experiments and the code is 220 mg/s. Therefore, the maximum production rate and total amount of hydrogen predicted by the code agree well with the experimental results.
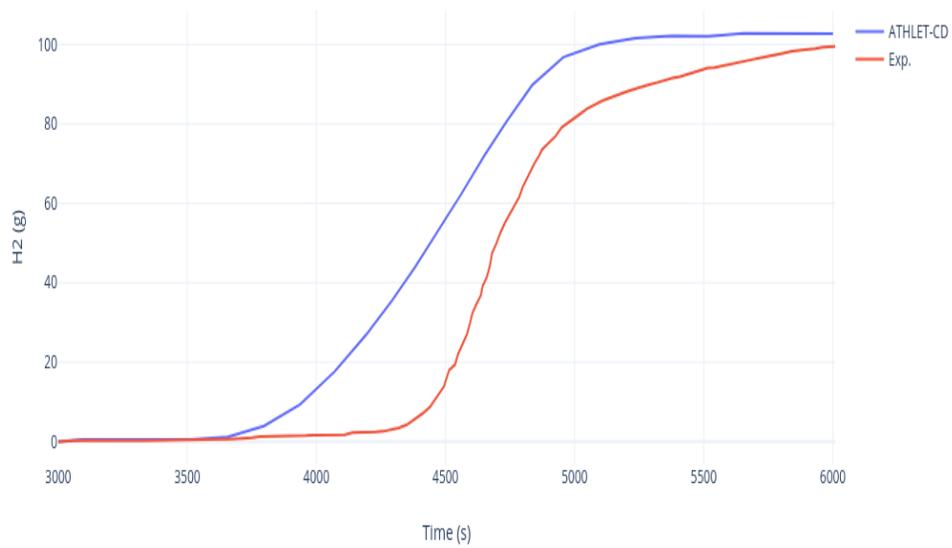
Figure 4.8 Total amount of hydrogen produced

5. CONCLUSION

In general, the code accurately simulates the test bundle's thermal behavior during the experiment. The calculated results mostly agree with the experimental data considering pre-oxidation phenomena. There are several factors observed during this study as a source of the differences between the measured data and predicted data. Some of those factors can be;

- assumptions made for the study,

- geometrical representation of the test facility (number of control volumes, location of junctions etc.),

- code structure,

- uncertainties in the modelling of melt relocation or material oxidation,

- challenges in modelling the quench cylinder.

The temperature rise in CORA-28 during the escalation was lower than in PWR bundle tests. The reason for this is that the zirconium high temperature water steam oxidation at the BWR bundles was much smaller. The PWR tests used 6 gram steam, while the BWR tests used 2 gram steam. In the BWR bundle testing, the lower reaction resulted in less hydrogen being produced. For the development of the ATHLET-CD, the code structure did not allow a distinction between heated and unheated rods, which means only one heat conduction object could be used for the fuel rods.

APPENDIX

THERMAL PROPERTIES OF MATERIALS

Table A.1. Thermal conductivity, λ [W/(mK)], of stoichiometric UO_2 fuel with 0.95 TD for burnup of 0 [11]

T (Kelvin)	Recommended		Referans
	0	0^a	0
673	4.74	3.85	4.71
773	4.28	3.57	4.23
873	3.89	3.43	3.84
973	3.55	3.35	3.52
1073	3.26	3.19	3.26
1173	3.01	2.99	3.03
1273	2.79	2.79	2.85
1373	2.61	2.61	2.69
1473	2.45	2.45	2.55
1573	2.32	2.32	2.44
1673	2.22	2.22	2.35
1773	2.14	2.14	2.28
1873	2.09	2.09	2.22
1973	2.06	2.06	2.19

Table A.1. Thermal conductivity, λ [W/(mK)], of stoichiometric UO2 fuel with 0.95 TD
for burnup of 0 [11] (cont.)

2073	2.06	2.06	2.17
2173	2.08	2.08	2.18
2273	2.12	2.12	2.21
2373	2.18	2.18	2.26
2473	2.26	2.26	2.34
2573	2.35	2.35	2.46
2673	2.45	2.45	2.61
2773	2.56	2.56	2.81
2873	2.68	2.68	3.07
2973	2.80	2.80	3.39
3073	2.93	2.93	3.79

[a] Radiation effect(Factor FR) with no burnup

Table A.2. Density and heat capacity of UO2 (Densities are for 100% TD fuel) [11]

Fuel	UO$_2$	
T(Kelvin)	$p*10^{-4}$ (kg/m^3)	C_p*10^{-2} (J/kg/K)
300	1.0961	2.3658
400	1.0929	2.6432
500	1.0897	2.8153

Table A.2. Density and heat capacity of UO2 (Densities are for 100% TD fuel) [11] (cont.)

600	1.0865	2.9299
700	1.0832	3.0071
800	1.0800	3.0584
900	1.0766	3.0918
1000	1.0733	3.1140
1100	1.0699	3.1306
1200	1.0664	3.1465
1300	1.0628	3.1666
1400	1.0590	3.1950
1500	1.0551	3.2357
1600	1.0551	3.2925
1700	1.0468	3.3688
1800	1.0423	3.4679
1900	1.0376	3.5926
2000	1.0327	3.7457
2100	1.0275	3.9297
2200	1.0220	4.1468
2300	1.0162	4.3989

REFERENCES

[1]   International Atomic Energy Agency, "Pre-oxidised BWR test CORA-28: Test results," June 1997. [Online]. Available: https://inis.iaea.org/search/search.aspx?orig_q=RN:29000256. [Accessed 6 October 2021].

[2]   Austregesilo, H., Bals, C., and Trambauer, K., "Post-test calculation and uncertainty analysis of the experiment Quench-07 with the System Code Athlet-CD," *Nuclear Engineering and Design*, pp. 1693–1703, 2007.

[3]   Josef Bestele, Klaus Trambauer & Johann-Dietrich Schubert, "Posttest Calculations of Bundle Quench Test CORA-13 with ATHLET-CD," *Nuclear Technology*, pp. 109-123, 1997.

[4]   Di Marcello, V., Imke, U., & Sanchez, V., "Validation and application of the System Code Athlet-CD for BWR severe accident analyses," *Nuclear Engineering and Design*, pp. 284–298, 2016

[5]   G. Lerchl, H. Austregesilo, A. Langenfeld, P. Schöffel, D. von der Cron, F. Weyermann., "ATHLET 3.2 User's Manual," GRS, 2019.

[6]   H. Austregesilo, C. Bals, T. Hollands, C. Köllein, L. Lovasz, W. Luther, P. Pandazis, J.-D. Schubert, L.Tiborcz, S. Weber, "ATHLET-CD MOD 3.2 USER MANUAL," GRS, 2019.

[7]   L. Lovasz, C. Bals, T. Hollands, C. Köllein, H. Aust-regesilo, P. Pandazis, L. Tiborcz, S. Weber, "ATHLET-CD MOD 3.2 Models and Methods Draft," GRS, 2019.

[8]   H. Austregesilo, C. Bals, A. Langenfeld, G. Lerchl, P. Schöffel, T. Skorek, D. Von der Cron, F. Weyermann., "ATHLET 3.2 Models and Methods," GRS, 2019.

[9]   Bernard Clément, Roland Zeyen, "The objectives of the Phébus FP experimental programme and main findings," *Annals of Nuclear Energy*, pp. 4-10, 2013.

[10]   Haste, T.; Steinbrück, M.; Barrachin, M.; de Luze, O.; Grosse, M.; Stuckert, J., "A comparison of core degradation phenomena in the CORA, QUENCH, Phebus SFD and Phebus FP experiments," KIT, 2013.

[11]   S. G. Popov, V. K. Ivanov, J. J. Carbajo, and G. L. Yoder,"THERMOPHYSICAL PROPERTIES OF MOX AND UO2 FUELS INCLUDING THE EFFECTS OF IRRADIATION," Nov-2000. [Online]. Available: https://info.ornl.gov/sites/publications/Files/Pub57523.pdf. [Accessed:Nov-2021].

[12]   J. Stuckert, H. Austregesilo, C. Bals, T. Hollands, A. Kiselev, D. Tomashchik, and T. Yudina, "Post-test analyses of the Cora-15 bundle test with the system codes Athlet-CD and Socrat," *Nuclear Engineering and Design*, vol. 342, pp. 320–335, 2019.

[13]   International Atomic Energy Agency, "Simulation of the Fuel Rod Bundle Test QUENCH-03 Using the System Codes ASTEC and ATHLET-CD", November 2010. [Online]. Available: https://inis.iaea.org/collection/NCLCollectionStore/_Public/48/026/48026397.pdf ?r=1&r=1. [Accessed 6 October 2021].

[14]   U.S. Department of Energy Office of Scientific and Technical Information, "Comparison of the quench experiments CORA-12, CORA-13, CORA-17", August 1996. [Online]. Available: https://www.osti.gov/etdeweb/biblio/417361. [Accessed 6 October 2021].

[15]   Hagen, S., Hofmann, P., Noack, V., Sepold, L., Schanz, G., Schumacher, G., "Pre-oxidised PWR test CORA-29: test results", Karlsruhe Institute of Technology, 1997.

[16]   Hagen, S., Hofmann, P., Noack, V., Sepold, L., Schanz, G., Schumacher, G., "Large bundle BWR test CORA-18: test results", Karlsruhe Institute of Technology, 1988.

[17]   Hagen, S., Hofmann, P., Noack, V., Sepold, L., Schanz, G., Schumacher, G., "BWR slow heatup test CORA-31: test results", Karlsruhe Institute of Technology, 1995.

VITA

Murat Tuter was born in Ankara, Turkey. He was awarded his Bachelor of Engineering in Mechanical Engineering from Ankara Yıldırım Beyazıt University, Turkey. He began his master's degree program in Nuclear Engineering at Missouri University of Science and Technology in January 2020. His master`s research was severe accident analysis on nuclear facilities. During his studies, he was sponsored by Ministry of National Education, Republic of Turkey and advised by Dr. Joshua Schlegel. He was the president of the Turkish Student Association at Missouri S&T. Finally, Murat Tuter received his Master of Science in Nuclear Engineering in May 2022 from Missouri University of Science and Technology, Rolla, Missouri, USA.